

Fundamental bounds on extraordinary transmission with experimental validation

Andrei Ludvig-Osipov^{1*}, Johan Lundgren², Casimir Ehrenborg², Yevhen Ivanenko³, Andreas Ericsson⁴,
Mats Gustafsson², B.L.G. Jonsson¹, and Daniel Sjöberg²

¹KTH Royal Institute of Technology, Stockholm SE-100 44, Sweden

²Lund University, Lund SE-221 00, Sweden

³Linnæus University, Växjö SE-351 95, Sweden

⁴TICRA, Landemærket 29, Copenhagen DK-1119, Denmark

Abstract—This paper presents a study of extraordinary transmission (EoT) through arrays of sub-wavelength apertures. Fundamental limitations for this phenomenon are formulated as a sum rule, relating the transmission coefficient over a bandwidth to the static polarizability. The sum rule is rigorously derived for arbitrary periodic apertures in thin screens. By this sum rule we establish a physical bound on the bandwidth of EoT which is verified numerically for a number of aperture array designs. We utilize the sum rule to design and optimize sub-wavelength frequency selective surfaces with a bandwidth close to the physically attainable. Finally, we verify the sum rule and simulations by measurements of an array of horseshoe-shaped slots milled in aluminum foil.

I. INTRODUCTION

Periodic sub-wavelength perforations in a metal screen can make the screen transparent to electromagnetic waves for certain frequency ranges, which depend on the geometry and periodicity of the perforations [1], [2], [3]. This is expected from the theory of diffraction for rather large perforations [4], [5], but it also holds true for perforations covering only a small fraction of the screen's area. For example, a metal screen with 5 % of its surface removed by perforations can be designed to have frequency bands with 80–100 % transmission level. Due to its nature, being both counter intuitive and contradictory to the classical theory of diffraction at optical frequencies [4], [5], this phenomenon is called *extraordinary transmission* (EoT). EoT was described two decades ago by Ebbesen et al. [1] for waves in the optical frequency range. Experimental studies and theoretical proposals describing the phenomenon have been presented *e.g.*, in [3], [2]. The same phenomenon was also observed and discussed for electromagnetic millimeter waves, see *e.g.*, [6], [7], and in acoustics [8].

From a theoretical perspective, EoT has been explained by surface plasmon polaritons at optical frequencies [2], [9], and by spoof plasmons at radio frequencies [10]. Alternative approaches to understanding this phenomenon include the theory of scattering by obstacles inside closed waveguides [7], impedance matching models [11], cavity resonances [12], and dynamical diffraction [13]. A simple interpretation of the EoT phenomenon, which is the one adopted throughout this paper, is that of a resonance of a periodic structure.

EoT applications include spatially tunable filters, near-field imaging and modulators as well as negative refractive index metamaterials [14]. In frequency selective surface (FSS) design the subwavelength apertures are commonly used [15]. A proposed FSS application is in slotted infrared-protective metalized windows [16]. These would be transparent for cell phone signals, to increase coverage inside of buildings, while serving as a barrier for infrared waves. Also, EoT structures localize high power flow within the apertures [17]. This effect can be additionally increased by designing apertures with narrow slots. This can be used to create nonlinear devices with strong concentration of fields. A further application is the Bethe-hole directional coupler [4], [5], where a periodic sequence of apertures in a wall joining two waveguides is designed to provide a coupling mechanism in the band of interest.

A limiting factor of EoT is that the frequency bands where the effect occurs are rather narrow. Naturally, it is desirable to understand the limitations of this effect; how much bandwidth is achievable and at what frequencies. The tuning of the EoT bandwidth is an iterative trial-and-error procedure, usually assisted by heuristically reasoned guidelines [15]. To facilitate this procedure, a physical bound in the form of a sum rule is proposed.

In this paper, we present a derivation of the EoT sum rule, which shows that the total EoT bandwidth is limited from above by the normalized static polarizability of the structure. We validate the sum rule by comparison both with simulated periodic structures, and also with measurements. We illustrate how the sum rule can be utilized in the design and bandwidth optimization of FSS. The sum rule is derived here for structures consisting of an infinitely thin perfect electric conductor (PEC) screen. We show by simulations that the transmitted power and bandwidth of a generic periodic design is not greatly affected by a finite thickness and conductivity up to certain limits. This motivates the use of the sum rule in evaluation of real structures as well as in a penalty function in optimization. A horseshoe slot aperture was designed and optimized utilizing the sum rule to maximize the transmission bandwidth in the lowest frequency peak. This design was manufactured in aluminum foil and measured in the frequency range 10 to 20 GHz.

The rest of the paper is organized as follows. Section II formulates the problem of scattering against periodic screens, and Section III gives a derivation of the sum rule for periodic structures. Numerical examples validating and illustrating the sum rule are presented in Section IV along with a demonstration of how the sum rule is used in the design process. Section V investigates the applicability of the sum rule for non-ideal structures. Section VI provides the details of the manufacturing process and the measurement setup, and presents the measured transmission coefficient, which is also compared to the theoretical predictions. Finally, the results of this paper are summarized and discussed in Section VII.

II. SCATTERING BY PERIODIC PERFORATED SCREENS

We consider the scattering of a linearly polarized electromagnetic plane wave by a periodically perforated metal screen in free space, see Figure 1. The goal is to quantify the amount of transmitted power that passes through the structure and continues to propagate as a wave of the same frequency, polarization and direction as the incident wave. To accomplish this, we extend the initial theoretical results reported in [18], and use them to impose a bandwidth bound on the power transmission of such structures. The theory is derived under the assumption that the structure is an infinitely thin two-dimensional periodic PEC screen of infinite extent in the plane normal to the incident wave direction. In Sections V and VI, these assumptions are validated to be reasonable approximations for power transmission through real structures.

The screen is placed in the xy -plane at $z = 0$, and the unit cell is defined by the lattice vectors $l_x \hat{x}$ and $l_y \hat{y}$. The incoming wave with the associated electric field $\mathbf{E}^{(i)}(k, \mathbf{r}) = E^{(i)} e^{i\mathbf{k} \cdot \mathbf{r}} \hat{e}$ is propagating in the positive z -direction, where \hat{e} is the polarization unit vector, $k = \omega/c$ is the wave number in free space with ω and c being the angular frequency and the speed of light in vacuum, respectively, $\mathbf{k} = k\hat{z}$ is the wavevector, \mathbf{r} is the field position vector, and the time convention $e^{-i\omega t}$ is used. Interaction between the incident wave and the structure gives rise to the scattered field. We denote the scattered field in $z < 0$ as the reflected field $\mathbf{E}^{(r)}(k, \mathbf{r})$, and the total field in $z > 0$ as the transmitted field $\mathbf{E}^{(t)}(k, \mathbf{r})$. A spectral decomposition of the transmitted field in Floquet modes is

$$\mathbf{E}^{(t)}(k, \mathbf{r}) = \sum_{m,n=-\infty}^{\infty} \mathbf{E}_{mn}^{(t)}(k) e^{i\mathbf{k}_{mn} \cdot \mathbf{r}}, \quad (1)$$

where $\mathbf{k}_{mn} = k_{x,n} \hat{x} + k_{y,m} \hat{y} + k_{z,mn} \hat{z}$ are the modal wave vectors with $k_{x,n} = 2\pi n/l_x$, $k_{y,m} = 2\pi m/l_y$, $k_{z,mn} = \sqrt{k^2 - k_{x,n}^2 - k_{y,m}^2}$ and $\mathbf{E}_{mn}^{(t)}(k)$ are the expansion coefficients. The latter are related to the incident field through a linear mapping

$$\mathbf{E}_{mn}^{(t)}(k) = \mathbf{T}_{mn}(k) \cdot \mathbf{E}^{(i)}(k, z=0), \quad (2)$$

where $\mathbf{T}_{mn}(k)$ are the transmission dyadic tensors. For frequencies below the first grating lobe, $f < c_0/\max\{l_x, l_y\}$ [15], only the fundamental mode is propagating. We define the co-polarized transmission coefficient for the fundamental mode as $T(k) = \hat{e} \cdot \mathbf{T}_{00}(k) \cdot \hat{e}$.

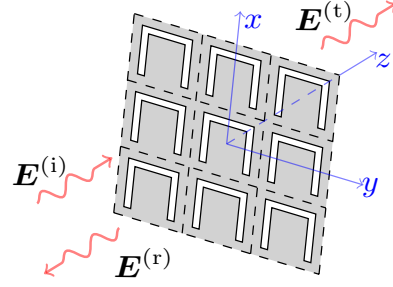


Fig. 1: A periodic planar array with normally incident (i), reflected (r) and transmitted (t) waves.

Given a transmission threshold T_0 we define the transmission bands as intervals of k , where $|T(k)| > T_0$. For the largest such interval (the main band) with endpoints k_1 and k_2 , the fractional bandwidth is

$$B = 2 \frac{k_2 - k_1}{k_1 + k_2}. \quad (3)$$

In this paper, we characterize how the fractional bandwidth depends on various perforation shapes with respect to different metrics, such as aperture area, or size of a minimal enclosing square, see S_p and a respectively, in Figure 2a. We strive towards having the bandwidth of the lowest-frequency transmission peak to be as large as possible.

III. DERIVATION OF THE SUM RULE

In this section, the derivation of the sum rule is presented. It is based on the passive properties of the screen [19], with an associated system response that can be transformed into a Herglotz function [20], [21], associated with the scattering system. An integral identity is applied to this function to obtain the extraordinary-transmission sum rule. The main theoretical result is the sum rule in (10), from which an upper bound of (3) is obtained in (12).

Passivity of the scattering configuration [19], [22], [23] allows an analytical extension of $T(k)$ for $k \in \mathbb{C}^+$, where $\mathbb{C}^+ = \{k \in \mathbb{C} : \text{Im } k > 0\}$ is the upper half plane. Apart from analyticity, a few additional properties are required to construct a physical bound in the form of a sum rule. The impinging wave generates electric currents on the screen. From the assumption of negligible thickness of the screen it follows that the scattered field is symmetric relative to the screen, i.e., $\mathbf{E}^{(t)} - \mathbf{E}^{(i)} = \mathbf{E}^{(r)}$ at $z = 0$. This can be rewritten as $T(k) = 1 + R(k)$, where $R(k)$ is the reflection coefficient defined for $\mathbf{E}^{(r)}$ similarly as $T(k)$ is defined for $\mathbf{E}^{(t)}$. This, combined with conservation of power $|T(k)|^2 + |R(k)|^2 \leq 1$, yields $|T(k) - 1/2| \leq 1/2$. Thus, the transmission coefficient is a holomorphic mapping from the upper complex half-plane \mathbb{C}^+ to the closed disc D with center at $1/2$ and radius $1/2$ in the complex plane, see the green disc in Figure 2b.

In order to obtain the sum rule, we transform the system response $T(k)$ in such a way that it becomes a Herglotz function, which is a mapping from the upper complex half-plane to its closure. Details about Herglotz functions and the associated integral identity used here are reviewed in Appendix A.

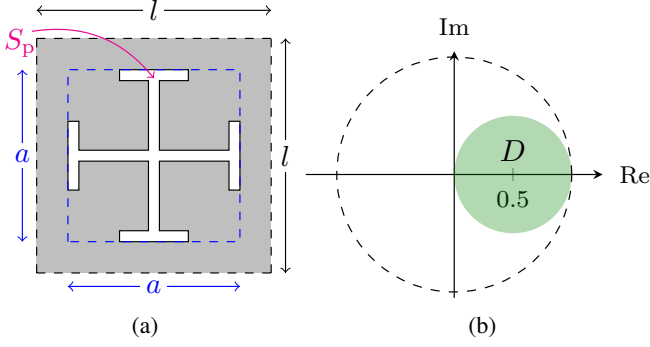


Fig. 2: (a) An example of the unit cell geometry, with perforated area S_p , contained in a minimal enclosing square of size a , and the unit cell size $l = l_x = l_y$; (b) Range of the transmission coefficient $T(k) \in D$ in the complex plane.

Here, we consider a Möbius transform [24], $m(\zeta) = i(1 - \zeta)/\zeta$, which maps the disc D to the closed upper complex half-plane. We compose it with the transmission coefficient to obtain a symmetric Herglotz function

$$g(k) = m(T(k)) = i \frac{1 - T(k)}{T(k)}. \quad (4)$$

A key element to derive the sum rule is the high and low frequency behavior of the transmission coefficient T , see (A.2) in Appendix A. To determine the low-frequency behavior we utilize Babinet's principle, the field $\mathbf{E}^{(t)}$ transmitted through an aperture screen and the field $\mathbf{E}_c^{(t)}$ transmitted through the complementary structure are related as $\mathbf{E}^{(t)} + \mathbf{E}_c^{(t)} = \mathbf{E}^{(i)}$ [25], [26], where $\mathbf{E}^{(i)}$ is the incident field in both cases, see also a single aperture case in [27]. Hence, the low-frequency expansion (i.e., $k \rightarrow 0$) can be found by investigating the complementary structure. In the complementary structure, the perforations are filled with perfect magnetic conductor (PMC) in the xy -plane and the PEC is removed. The transmission coefficient of the complementary structure is $T_c(k) = 1 - T(k)$ [27]. Its low-frequency expansion is [23], [28], [29], [30]

$$T_c(k) \sim 1 + \frac{ik\gamma}{2A} \quad \text{as } k \rightarrow 0, \quad (5)$$

where $\gamma = (\hat{\mathbf{e}} \cdot \boldsymbol{\gamma}_e \cdot \hat{\mathbf{e}} + (\hat{\mathbf{k}} \times \hat{\mathbf{e}}) \cdot \boldsymbol{\gamma}_m \cdot (\hat{\mathbf{k}} \times \hat{\mathbf{e}}))$, $\hat{\mathbf{k}} = \hat{\mathbf{z}}$ is the wave propagation direction, $\boldsymbol{\gamma}_e$ and $\boldsymbol{\gamma}_m$ are the electric and the magnetic polarizability tensors of the complementary structure, respectively, and $A = l_x l_y$ is the area of the unit cell. This gives us the expansion for the perforated PEC screen

$$T(k) \sim -\frac{ik\gamma}{2A} \quad \text{as } k \rightarrow 0. \quad (6)$$

Note that the polarizabilities used here are the polarizabilities for the complementary structure. Furthermore, for a planar PMC array and the electric field direction $\hat{\mathbf{e}}$ parallel to the array plane, the term $\hat{\mathbf{e}} \cdot \boldsymbol{\gamma}_e \cdot \hat{\mathbf{e}}$ vanishes, and thus we only need to calculate the magnetic polarizability. The magnetic polarizability of a PMC structure can be calculated as the electric polarizabilities of a PEC structure of the same shape, see e.g., [23], [31].

To construct the desired sum rule, we apply a Herglotz function with specific properties to $g(k)$ in (4). The resulting function will be a Herglotz function, as non-zero Herglotz functions satisfy the property that a composition of two Herglotz functions is a Herglotz function [20]. To obtain an effective sum rule, we want to characterize the total attainable bandwidth. To do this, we need to emphasize the bands where the transmission is higher than a chosen threshold T_0 and to disregard the rest of the spectrum. The desired function h_Δ should have the properties $\text{Im } h_\Delta(g(k)) = 1$ when $|T| \geq T_0$ and zero otherwise. The pulse Herglotz function [20]

$$h_\Delta(\zeta) = \frac{1}{\pi} \ln \frac{\zeta - \Delta}{\zeta + \Delta} \sim \begin{cases} i & \text{as } \zeta \rightarrow 0 \\ -\frac{2\Delta}{\pi\zeta} & \text{as } \zeta \rightarrow \infty, \end{cases} \quad (7)$$

satisfies these criteria and has previously been used to construct sum rules for passive metamaterials [32] and high-impedance surfaces [29]. For any real-valued argument x this function has the property $\text{Im } h_\Delta(x) = 1$ for $|x| < \Delta$ and $\text{Im } h_\Delta(x) = 0$ for $|x| > \Delta$. We use this property later to relate the resulting integral identity with the fractional bandwidth (3) for the lossless case. For the composed function $h_\Delta(g(k))$, the connection between the parameter Δ and the threshold T_0 is found from relating Δ to a threshold value of $g(k)$ (i.e. when $|T(k)| = T_0$)

$$\Delta^2 = \frac{1 - T_0^2}{T_0^2}. \quad (8)$$

Finally, we apply the integral identity (A.2) to the function $h_\Delta(g(k))$. From (6) we obtain that $T(k) \sim -ik\gamma/(2A)$ for $k \rightarrow 0$. Combining this result and the low-frequency asymptote of (4), we get $g(k) \sim -2A/(\gamma k)$ as $k \rightarrow 0$. Consequently, the function $h_\Delta(g(k))$ has the low-frequency expansion $h_\Delta(g(k)) \sim k\gamma\Delta/(A\pi)$ for $k \rightarrow 0$. Performing the same steps for the high frequency limit yields $h_\Delta(g(k)) \sim o(k)$ as $k \rightarrow \infty$. Thus, according to (A.2) we find the sum rule

$$\int_0^\infty \frac{\text{Im } h_\Delta(g(k))}{k^2} dk = \frac{\gamma\Delta}{2A}. \quad (9)$$

After substituting $\lambda = 2\pi/k$ and reusing $g(\lambda)$ for (4) as a function of wavelength, an alternative form of the sum rule is

$$\int_0^\infty \text{Im } h_\Delta(g(\lambda)) d\lambda = \frac{\gamma\Delta\pi}{A}. \quad (10)$$

From this sum rule expression we deduce the upper bound of (3) convenient for practical use. The sum rule shows that the total sum of transmission bands of an aperture array is determined by the array's polarizability per unit area. Note that the right-hand side of (10) is always strictly positive and hence there must exist intervals with non-zero transmission. Moreover, the transmission is perfect ($|T(\lambda_0)| = 1$) for some wavelength λ_0 if the structure is resonant below the onset of grating lobes and the cross polarization is negligible. This is a consequence of a lossless scattering system ($|T|^2 + |R|^2 = 1$) for which T is located on the boundary circle of D , in Figure 2b. This implies that $\text{Im } h_\Delta(g(\lambda)) = 1$ for some wavelength interval of nonzero length, i.e., there always exists

a transmission band with an arbitrarily high level of transmission.

Note that, although ohmic losses are eliminated for screens made of PEC material the scattering system is in general lossy due to radiation in other modes than the co-polarized fundamental mode in (2). Such radiation is perceived as losses from the system point of view, and includes higher-order modes radiating above the grating lobe frequency, as well as the cross-polarized mode below the first grating lobe. We refrain here from considering lossy materials from a theoretical perspective, which is given in [18], as the resulting lossy case bound is in general not tight. Instead, we treat our lossless PEC model as an approximation of a highly conductive low-loss screen. Further discussion on the validity of the model is provided in Sections V-VI.

For practical applications the integration over a finite interval of wavelengths $[\lambda_a, \lambda_b]$ is performed (*e.g.*, see Figure 3 with $[\lambda_a, \lambda_b] = [0.6l, 5.2l]$, where l is the unit cell size)

$$\int_{\lambda_a}^{\lambda_b} \text{Im } h_{\Delta}(g(\lambda)) d\lambda \leq \frac{\gamma\pi\Delta}{A}. \quad (11)$$

Assume now that within the interval $[\lambda_a, \lambda_b]$ there are a number of mutually disjoint subintervals, where $|T| \geq T_0$. As an example, in Figure 3 we observe two intervals for $\lambda/l > 0.9$ with transmission higher than $T_0 = 0.8$, where the widest is located around $\lambda/l = 3$. In this paper, we focus mainly on the bandwidth of the widest transmission band. If we retain only the contribution of the largest transmission band with endpoints λ_1 and λ_2 , and normalize (11) with the central wavelength $\lambda_0 = (\lambda_1 + \lambda_2)/2$ of the corresponding band, we obtain a bound for the fractional bandwidth

$$B = 2 \frac{\lambda_1 - \lambda_2}{\lambda_1 + \lambda_2} \leq \frac{\gamma\pi\Delta}{A\lambda_0}. \quad (12)$$

IV. NUMERICAL EXAMPLES AND APPLICATIONS OF THE BOUND

We begin this section with illustrating the sum rule (10) by analyzing a given FSS design. The numerical example in Figure 3 shows the transmittance $|T|^2$ through an array of cross-potent (sometimes referred to as Jerusalem cross) [33], [15] shaped apertures as a function of the normalized wavelength. The assumptions of the idealized model are retained: the screen is infinitely thin and made of PEC material, and the array of perforations is infinitely periodic. The unit cell geometry is given, with $l_x = l_y = l$, slot width $w = l/20$, and parameters $a = 0.9l$ and $b = 0.4l$. The numerical analysis was performed in CST MW Studio using the frequency domain solver and Floquet mode ports. The results show the main transmission band (transmittance threshold level $|T_0|^2 = 0.8$) centered at $\lambda = 2.9l$, with the fractional bandwidth $B = 0.24$. This accounts for 86% of the upper bound limit in (12). For the wavelengths shorter than 0.9λ , we observe multiple narrower peaks. Due to the resonance nature of the phenomenon, an infinite number of such peaks is expected in the short wavelength limit. The contributions from these peaks, along

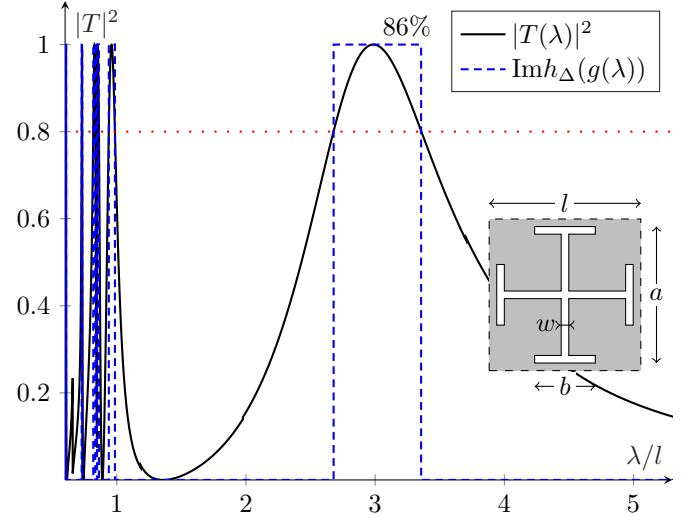


Fig. 3: Cross potent: transmittance as a function of wavelength and the unit cell geometry. Transmission bands with respect to the threshold level T_0^2 (dotted line) are shown by the integrand function $\text{Im } h_{\Delta}(g(\lambda))$ of (10).

with the grating lobes, are also accounted for in the left hand side of the sum rule (10).

In the above cross-potent example, the sum-rule is used to analyze a given FSS design. Additionally, the sum rule is instrumental to design and optimize FSS, which we discuss and illustrate in the remainder of this section. One of the most crucial performance parameters of a periodically perforated screen is the frequency bandwidth over which the screen is transparent. The bandwidth optimization of periodic screens typically involves a considerable amount of full-wave numerical simulations in order to tune the design. Thus, tools that guide the optimization process and reduce the number of simulations are desired. The sum rule (12) is such a tool, as it provides a quantitative estimate of the total attainable bandwidth. This can be used in two ways. First, the total attainable bandwidth is bounded by the static polarizability of a perforation element according to (12). Testing the static polarizability for each design candidate can thus replace numerically costly wide-frequency-range full-wave simulations in the search of preliminary structure. Second, the total attainable bandwidth, obtained from the polarizability, can serve as a reference for the fraction of the total bandwidth in the main frequency band. Using this reference, we can optimize the main frequency band to utilize most of the physically attainable bandwidth. In this section we demonstrate an optimization procedure by maximizing the frequency bandwidth of EoT through a perforated screen, while keeping the area of perforations S_p low (1 – 5% of the total screen area). In general, different metrics can be considered instead of S_p , for example, the size of the smallest enclosing square.

The total achievable EoT bandwidth is determined by the polarizability of the corresponding complementary structure according to (12), as discussed above. We use this as a guideline to choose the preliminary perforation design. Figure 4

compares the normalized polarizability γ/l^3 of an array of square PEC patches of size $a \times a$ and period $l_x = l_y = l$ with periodic PEC arrays, tightly enclosed by the square patch structure. Three shapes of enclosed unit cell designs are considered: a cross potent, a horseshoe and a split ring resonator. According to the monotonic growth of polarizabilities with volume, the polarizability of an enclosed object cannot exceed the polarizability of an enclosing object [34]. Thus, the polarizability of the square patches is the upper bound for the enclosed designs. We observe in Figure 4 that the horseshoe and the split ring designs approach the upper bound, and thus make a good use of the unit cell geometry. The split-ring-resonator unit cell outperforms the horseshoe-shaped design when they are compared with respect to normalized distance $(l - a)/l$ between the adjacent perforations.

As an alternative evaluation of performance we can investigate how the shapes perform with respect to the perforation area. Figure 5 shows the normalized static polarizability γ/l^3 as a function of the percentage of perforation area in the total area of the screen $\alpha = S_p/A$, where $l = l_x = l_y$ is the size of a unit cell, see Figure 2a. Here, solid, \circ -dashed, \square -dashed and \star -dashed lines correspond to square hole, cross potent, horseshoe and split ring resonator designs, respectively. All the designs were contained within the square of size a , and the slot width for the cross potent, horseshoe and split ring was fixed at $w = a/17$, see *e.g.*, Figures 3 and 6, while the unit cell size l was varied in the range $[1.03a, 11.15a]$, $[1.04a, 4.67a]$, $[1.03a, 4.12a]$ and $[1.38a, 6.17a]$ for the corresponding design, respectively. The evaluation of static polarizabilities was performed via a variational approach [30] in COMSOL Multiphysics electrostatic solver.

We observe among all considered shapes that the horseshoe utilizes the perforation area better than the other shapes, in the sense of the upper bound γ/l^3 of the total attainable bandwidth. The square hole perforations are given as a reference, and all the suggested designs outperform it. The same total bandwidth, as achieved by cutting out 15% of the screen with square-shaped perforations, can be attained by cutting out only 2.5% of the screen with the horseshoe-shaped perforations. Additionally, the horseshoe-shaped perforations have better mechanical stability compared to the other considered designs, which finalizes the choice of the preliminary structure.

Having chosen a horseshoe design as a preliminary structure, we perform optimization of its geometrical parameters with respect to its transmission bandwidth. Consider the following optimization problem. For a given upper limit α_0 of $\alpha = S_p/A$, make the fractional bandwidth B as close as possible to its upper bound given by the right hand side of (12). We denote the ratio between the bandwidth and its upper bound as $\eta(\Omega, \Delta) = B/(\gamma\pi\Delta/A\lambda_0)$. The optimization problem is formulated as follows for a given Δ

$$\begin{aligned} & \underset{\Omega}{\text{maximize}} && \eta(\Omega, \Delta) \\ & \text{subject to} && \alpha(\Omega) \leq \alpha_0, \end{aligned} \quad (13)$$

where optimization is performed over the parametrized geometry Ω of the aperture. We use a genetic algorithm optimization

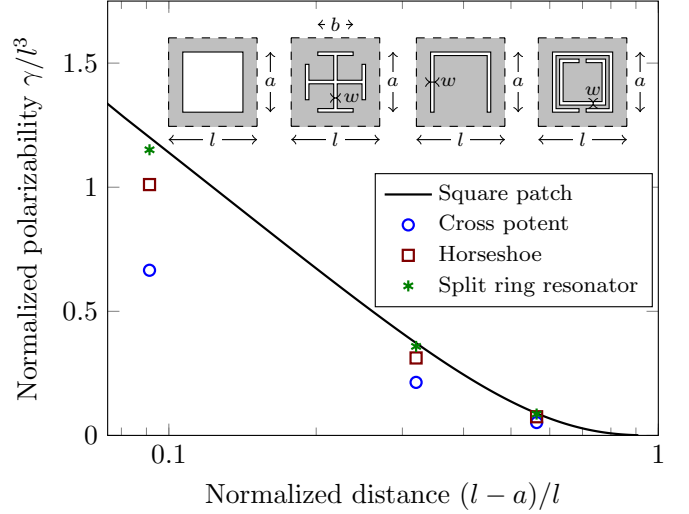


Fig. 4: Normalized polarizability γ/l^3 of infinitely thin PEC periodic structures as a function of the normalized distance between two adjacent square patches, $l \in \{1.1a, 1.47a, 2.29a\}$. The external applied field for polarizability calculation is directed vertically with respect to the unit cells in the inset.

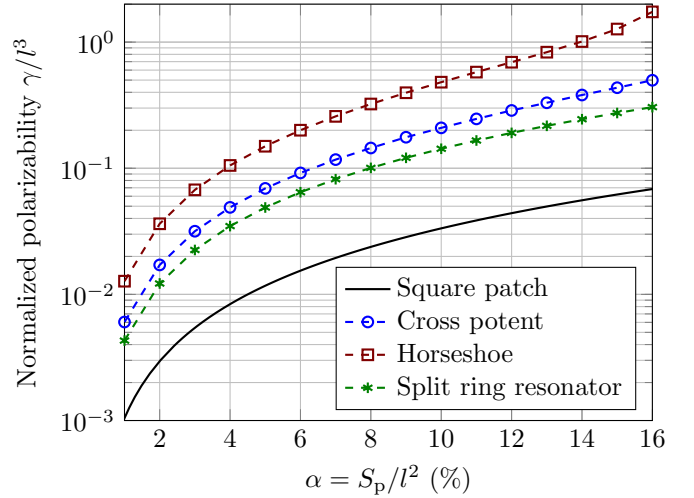


Fig. 5: Normalized polarizability γ/l^3 of infinitely thin PEC periodic structures as a function of perforated area. The external applied field for polarizability calculation is directed vertically with respect to the unit cells in the inset of Figure 4.

for geometric parameters of a horseshoe shaped aperture (the shape choice is motivated by Figure 5).

Figure 6 shows the results of optimization of the horseshoe perforation geometry with $\alpha_0 = 5\%$. We start with non-optimized design given by the size a , and $l = 1.69a$, $w_1 = w_2 = 0.049a$. Optimization (13) yields the design given by $l = 1.43a$, $w_1 = 0.049a$, and $w_2 = 0.0047a$. We observe that the bandwidth is improved approximately twice, and the main peak contains 96% of the attainable bandwidth, according to (12).

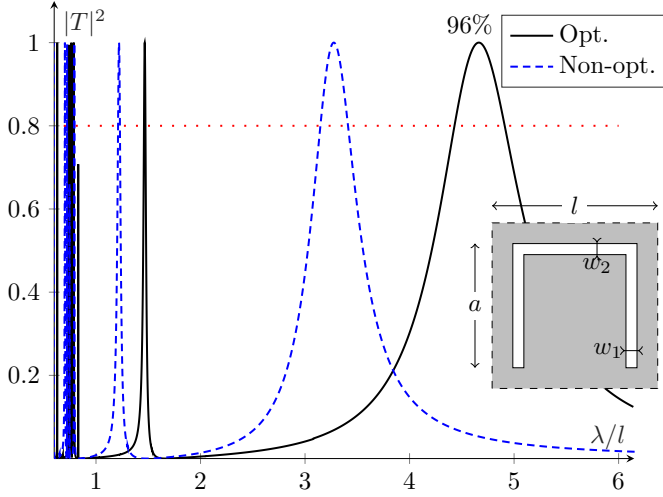


Fig. 6: Horseshoe transmittance, optimized (black curve) and non-optimized (dash-dotted) designs. In both cases $\alpha = S_p/A = 5\%$.

V. IMPLEMENTATION OF REAL STRUCTURES

In Sections II–IV, the theoretical and numerical evaluation of the screen were performed under certain assumptions. Here, we investigate the validity of these results when the assumptions are relaxed. One of the key assumptions was that the screen is infinitely thin. Figure 7 illustrates how the screen thickness d affects the screen's transmission characteristics. We consider transmission through a screen with horseshoe-shaped apertures, with slot width $w_1 = w_2 = w$, see Figure 6 for the unit cell geometry. The transmission through an infinitely thin screen is compared with three screens width-to-thickness ratios $w/d = \{1, 5, 10\}$. For $w/d = 1$, we observe a noticeable bandwidth reduction in comparison with the infinitely thin case. However, when $w/d = 10$, the difference between the transmittance of the infinitely thin screen and the screen of thickness d is negligible, resulting in a bandwidth reduction of about 2% (with the threshold ($|T_0|^2 = 0.8$)). Figure 7 shows that transmission bandwidth is reduced with decreasing w/d ratio. This implies that the inequality in (12) is still valid for cases with a finite thickness. However, when the slot width becomes comparable to the slot thickness, the bound is not tight.

The second crucial assumption made in the derivation of the sum rule was the PEC material of the screen. Therefore, candidates for screen material should be highly conductive low-loss metals. To reconcile this requirement with limitations put on thickness and mechanical stability, aluminum foil was chosen. Alternative options were metalized dielectric substrate, copper sheet and silver foil. However, these options impose issues which are hard to resolve in the sum rule or fabrication. Figure 8 shows the simulated transmittance for a perforated screen made of PEC or aluminum. The geometrical parameters of the screen are the same as of the manufactured sample, to be discussed in the next section. The aluminum screen has slightly lower amplitude (about 5%) in the transmission peak in comparison with the PEC screen. However, the bandwidth

reduction is negligible. Thus, the sum rule is applicable to aluminum screens and it is relatively tight.

In the sum rule we also considered an infinite periodicity of the screen. Ref. [35] reports that 30 periods in both dimensions of the screen is sufficient to ensure a negligible difference in transmission between finite and infinite structures. The edge effects can be compensated by time-gating.

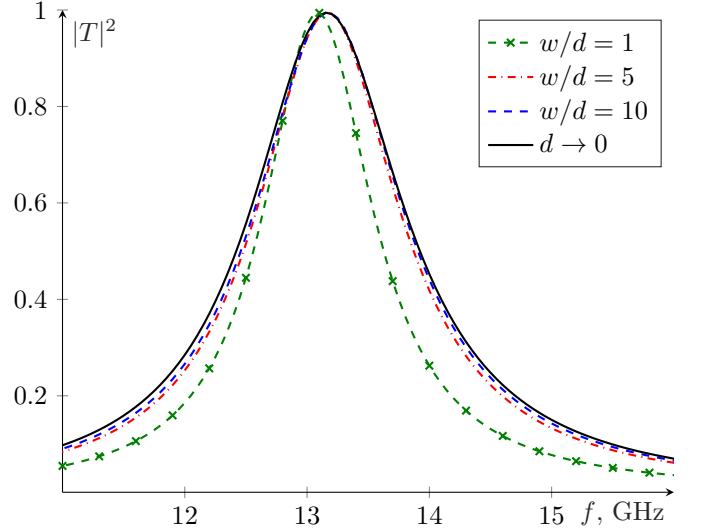


Fig. 7: Simulated transmittance through an array of horseshoe apertures for different ratios of the slot width to the screen thickness.

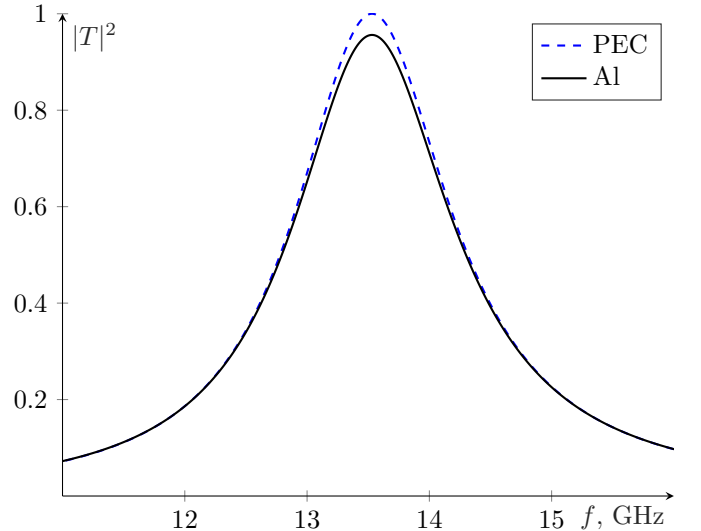


Fig. 8: Simulated transmittance of the horseshoe design for manufactured sample, PEC and Al comparison.

VI. MEASUREMENTS

The final manufactured sample had the unit cell geometry given by the inset in Figure 6 with $l = 6.57$ mm, $a = 3.43$ mm, $w_1 = 0.3$ mm, and $w_2 = 0.06$ mm. The aperture array was laser milled by a ProtoLaser U3 machine in a sheet of aluminum foil of thickness $d = 0.018$ mm. The array

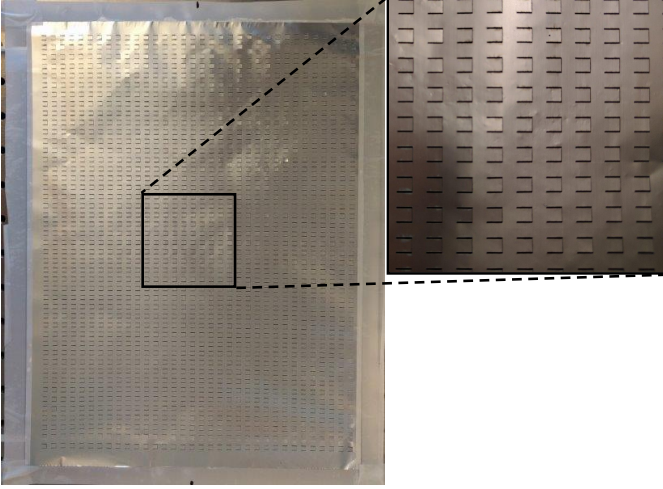


Fig. 9: Sample manufactured in aluminium foil: the entire sample of the size $238\text{ mm} \times 320\text{ mm}$ and a close up of the manufactured horseshoe design.

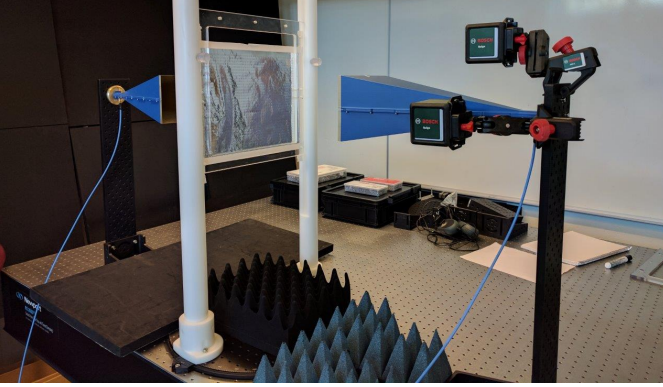


Fig. 10: Measurement setup mounted on an optical table. Two blue standard gain, horn Satimo SGH1240 antennas were used as both receiver and transmitter. The horns were aligned using two Bosch Quigo Cross line lasers, seen here mounted on the right antenna. The sample was mounted on a custom made polymethyl methacrylate frame and held up by two plastic stands.

consisted of $34 \times 45 = 1530$ apertures, and $\alpha = 5\%$. See Figure 9 for the manufactured sample.

The measurement setup is shown in Figure 10. The sample was fixed in a polymethyl methacrylate (PMMA) frame fastened by two plastic stands equidistant to the transmitting and receiving antennas. Standard gain horn Satimo SGH1240 antennas were used, with the nominal frequency range $12.4 - 18.0\text{ GHz}$. The antennas were installed at the distance 1 m from each other. The reference transmission measurements were performed with the empty PMMA frame instead of the sample and multipath reflections from the surrounding objects and surfaces were filtered out in the time domain by using time-gating [36], [37] utilizing a tapered cosine window.

The transmission through the manufactured sample was measured in the frequency range $10 - 20\text{ GHz}$ to capture the first transmission peak and to filter multipath components in an

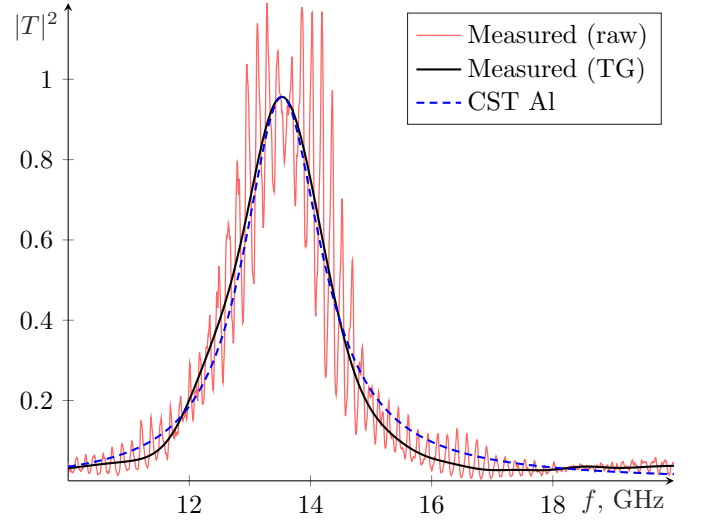


Fig. 11: Horseshoe slot array: comparison between measured raw data (red), processed data (black solid) and simulated (blue dashed) transmittance.

efficient manner. In Figure 11, the red and black solid curves correspond to the raw data of the measured transmittance and the processed data obtained by filtering out multipath propagation components using time gating, respectively, and the dashed curve corresponds to the simulated transmittance of the infinitely-periodic model of the sample. We observe a fine agreement between the measured and simulated transmittances in the whole frequency range. The magnitude and the frequency of the resonance perfectly coincide for simulation and measurements.

The optimized PEC-bandwidth of the lowest-frequency peak, as shown in Section IV, reaches 96% of the available physical bandwidth, based on the sum rule utilizing the polarizability of the perforation (12). As we saw in Section V, a finite thickness, but small in comparison with the perforation size, together with a finite but high conductivity made small perturbations to the transmission peak.

By comparing the measured result with the PEC-simulated results at the 80% transmittance threshold level, we find that the time-gated measured transmission peak has 98% of the available bandwidth of a PEC-based structure. The measured transmission peak is centered at the frequency of 13.52 GHz with the fractional bandwidth of 5.83%.

The remarkable similarity between measured and PEC-simulated results validate the use of the PEC-based sum rule as a tool to predict the physically maximally available bandwidth in thin and highly conductive EoT-screens. We further notice that the PEC-based upper bound solely utilizes the observation that the screen is a passive system.

VII. CONCLUSIONS

In this paper we have revisited the sum rule for periodic structures and applied it to an extraordinary transmission problem. We show numerically, that a periodic PEC-like infinitely thin screen with 5% of its total area cut out as horseshoe

shaped perforations can have up to 96% of its physically attainable bandwidth in its largest transmission window. The transmittance threshold of this study was set to 80%. Our numerical investigations illustrate that small perturbations of the PEC-screen accounting for a finite thickness and a finite but high conductivity marginally perturbed the EoT-transmission result. This indicates the validity of the sum rule for real applications, even though it was derived for an ideal model.

We experimentally validate our results by showing that the transmission characteristics of the first transmission window of a horseshoe design, optimized with the use of the sum rule, fabricated in a 0.018 mm thick highly conducting aluminum foil with horseshoe perforations, accurately matches the corresponding simulations. The mutual agreement between the theoretical limitations, numerical and experimental validation is high. The choice of frequency band was selected to fully utilize the range of the experimental equipment. We conclude that the sum rule can be used to predict the results of EoT-experiments with highly conductive metal films in the GHz range, and may be of use in understanding the phenomena at other frequencies. We also observe that the perforation shape needed to maximize the performance of this phenomenon can be rather simple and still gather a high degree of transmission in one transmission window.

The theoretical sum rule result (10) shows that a transmission band at long (in comparison to the periodicity of the structure) wavelengths exists for any type of perforations, even infinitely small ones ($\alpha \rightarrow 0$). However, the bandwidth of the transmission peak is proportional to the polarizability, closely related to the shape and size of the perforations. As a result, it is shown that the static polarizability, and hence, the transmission bandwidth of an array of square apertures can be attained by periodic perforations of much smaller relative area α , see Figures 4 and 5. This provides a theoretical ideal model perspective on the earlier works [1], [3], investigating the ratio of transmission level to perforation area T/α of a transmission peak by experiment or real-material model. The sum rule (10) implicates that in the ideal setting the ratio T/α can be infinitely large.

The good agreement between the measured transmission peak and the corresponding PEC simulations was enabled by a careful choice of material. By utilizing aluminum foil we stayed relatively close to the idealized PEC case. There was no dielectric material supporting the metal, and the foil had high conductivity, which ensured a high value of in the transmission peak. The foil was also thinner than the smallest slot in the design. This meant that there was no waveguide-like phenomenon occurring in the slots. Such an effect has a tendency to shift the spectral localization of resonances. This can be compared to the initial investigation performed at optical frequencies [1], [2], [3], where the aperture sizes are small compared to the thickness of the materials they are etched in. This explains why these studies exhibit deviations from ideal models.

APPENDIX A HERGLOTZ FUNCTIONS

A Herglotz function is a holomorphic function $h(\zeta)$ such that $\text{Im } h(\zeta) \geq 0$ whenever $\text{Im } \zeta > 0$, i.e., it is a mapping from the upper complex half plane to its closure. Functions of this class can have a family of integral identities [20], also known as sum rules.

Consider a Herglotz-function such that

$$h(\zeta) = \begin{cases} a_{-1}\zeta^{-1} + a_1\zeta + o(\zeta) & \text{as } \zeta \rightarrow 0, \\ b_1\zeta + o(\zeta^{-1}) & \text{as } \zeta \rightarrow \infty, \end{cases} \quad (\text{A.1})$$

where the coefficients a_{-1} , a_1 and b_1 are real-valued. Here $\zeta = x + iy$. A sum rule [20], [21] for the Herglotz function h with the above expansion is:

$$\frac{2}{\pi} \int_{0+}^{\infty} \frac{\text{Im } h(x)}{x^2} dx \stackrel{\text{def}}{=} \lim_{\varepsilon \rightarrow 0+} \lim_{y \rightarrow 0+} \frac{2}{\pi} \int_{\varepsilon}^{1/\varepsilon} \frac{\text{Im } h(x + iy)}{x^2} dx = a_1 - b_1. \quad (\text{A.2})$$

Above, \rightarrow denotes the limit in a cone $\alpha \leq \arg(\zeta) \leq (\pi - \alpha)$ for some $\alpha > 0$. Throughout this paper, we utilize the symmetry $h(\zeta) = -h^*(-\zeta^*)$, which follows from the real-valuedness of the function in the time domain.

ACKNOWLEDGMENT

We are grateful to Martin Nilsson for aiding in the sample manufacturing process. The authors acknowledge the support of the Swedish foundation for strategic research (SSF) under the grant ‘Complex analysis and convex optimization for electromagnetic design’.

REFERENCES

- [1] T. W. Ebbesen, H. J. Lezec, H. F. Ghaemi, T. Thio, and P. A. Wolff, “Extraordinary optical transmission through sub-wavelength hole arrays,” *Nature*, vol. 391, pp. 667–669, 1998.
- [2] K. J. K. Koerkamp, S. Enoch, F. B. Segerink, N. F. van Hulst, and L. Kuipers, “Strong influence of hole shape on extraordinary transmission through periodic array of subwavelength holes,” *Phys. Rev. Lett.*, vol. 92, no. 18, p. 183 901, 2004.
- [3] L. Martín-Moreno, F. J. García-Vidal, H. J. Lezec, K. M. Pellerin, T. Thio, J. B. Pendry, and T. W. Ebbesen, “Theory of extraordinary optical transmission through subwavelength hole arrays,” *Phys. Rev. Lett.*, vol. 86, pp. 1114–1117, 6 2001.
- [4] H. A. Bethe, “Theory of diffraction by small holes,” *Phys. Rev.*, vol. 66, pp. 163–182, 7-8 1944.
- [5] T. K. Ishii, *Handbook of microwave technology*, Elsevier, 1995.
- [6] M. Beruete, M. Sorolla, I. Campillo, J. S. Dolado, L. Martín-Moreno, J. Bravo-Abad, and F. J. García-Vidal, “Enhanced millimeter-wave transmission through subwavelength hole arrays,” *Opt. Lett.*, vol. 29, no. 21, pp. 2500–2502, 2004.
- [7] F. Medina, F. Mesa, and R. Marques, “Extraordinary transmission through arrays of electrically small holes from a circuit theory perspective,” *IEEE Transactions on Microwave Theory and Techniques*, vol. 56, no. 12, pp. 3108–3120, 2008.
- [8] M.-H. Lu, X.-K. Liu, L. Feng, J. Li, C.-P. Huang, Y.-F. Chen, Y.-Y. Zhu, S.-N. Zhu, and N.-B. Ming, “Extraordinary Acoustic Transmission through a 1D Grating with Very Narrow Apertures,” *Phys. Rev. Lett.*, vol. 99, p. 174 301, 17 2007.
- [9] C. Genet and T. W. Ebbesen, “Light in tiny holes,” *Nature*, vol. 445, pp. 39–46, 2007.
- [10] J. B. Pendry, L. Martín-Moreno, and F. J. García-Vidal, “Mimicking surface plasmons with structured surfaces,” *Science*, vol. 305, no. 5685, pp. 847–848, 2004.

- [11] A. Alú, G. D'Aguanno, N. Mattiucci, and M. J. Bloemer, "Plasmonic brewster angle: Broadband extraordinary transmission through optical gratings," *Phys. Rev. Lett.*, vol. 106, p. 123 902, 12 2011.
- [12] Q. Cao and P. Lalanne, "Negative role of surface plasmons in the transmission of metallic gratings with very narrow slits," *Phys. Rev. Lett.*, vol. 88, p. 057 403, 2002.
- [13] M. M. J. Treacy, "Dynamical diffraction in metallic optical gratings," *Appl. Phys. Lett.*, vol. 75, pp. 606–608, 5 1999.
- [14] C. García-Meca, R. Ortuño, F. Rodríguez-Fortuño, J. Martí, and A. Martínez, "Negative refractive index metamaterials aided by extraordinary optical transmission," *Opt. Express*, vol. 17, no. 8, pp. 6026–6031, 2009.
- [15] B. A. Munk, *Frequency selective surfaces: Theory and design*, Wiley, 2000.
- [16] M. Gustafsson, A. Karlsson, A. P. P. Rebelo, and B. Widenberg, "Design of frequency selective windows for improved indoor outdoor communication," *IEEE transactions on antennas and propagation*, vol. 54, no. 6, pp. 1897–1900, 2006.
- [17] M. Beruete, M. Sorolla, and I. Campillo, "Left-handed extraordinary optical transmission through a photonic crystal of subwavelength hole arrays," *Optics Express*, vol. 14, no. 12, pp. 5445–5455, 2006.
- [18] M. Gustafsson, D. Sjöberg, and I. Vakili, "On the extraordinary transmission through sub-wavelength apertures in perfectly conducting sheets," *2011 International Conference on Electromagnetics in Advanced Applications*, pp. 1233–1236, 2011.
- [19] A. H. Zemanian, *Distribution theory and transform analysis: An introduction to generalized functions, with applications.*, Courier Corporation, 1965.
- [20] A. Bernland, A. Luger, and M. Gustafsson, "Sum rules and constraints on passive systems," *J. Phys. A: Math. Theor.*, vol. 44, p. 145 205, 2011.
- [21] M. Nedic, C. Ehrenborg, Y. Ivanenko, A. Ludvig-Osipov, S. Nordebo, A. Luger, B. L. G. Jonsson, D. Sjöberg, and M. Gustafsson, "Herglotz functions and applications in electromagnetics," in *Advances in Mathematical Methods for Electromagnetics*, K. Kobayashi and P. Smith, Eds. IET, 2018.
- [22] H. M. Nussenzveig, *Causality and dispersion relations.*, Academic Press, London, 1972.
- [23] M. Gustafsson, C. Sohl, C. Larsson, and D. Sjöberg, "Physical bounds on the all-spectrum transmission through periodic arrays," *EPL (Europhysics Letters)*, vol. 87, no. 3, p. 34 002, 2009.
- [24] J. B. Conway, *Functions of one complex variable*, Springer, New York, NY, 1973.
- [25] L. D. Landau, E. M. Lifshitz, and L. P. Pitaevskii, *Electrodynamics of continuous media*. Pergamon, 1984.
- [26] J. van Bladel, *Electromagnetic fields*. IEEE Press, 2007.
- [27] M. Gustafsson, "Sum rule for the transmission cross section of apertures in thin opaque screens," *Opt. Lett.*, vol. 34, pp. 2003–2005, 2009.
- [28] R. E. Kleinman and T. B. A. Senior, *Low and high frequency asymptotics*. Elsevier Science, 1986.
- [29] M. Gustafsson and D. Sjöberg, "Physical bounds and sum rules for high-impedance surfaces," *IEEE Transactions on Antennas and Propagation*, vol. 59, no. 6, pp. 2196–2204, 2011.
- [30] D. Sjöberg, "Variational principles for the static electric and magnetic polarizabilities of anisotropic media with perfect electric conductor inclusions," *Journal of Physics A: Mathematical and Theoretical*, vol. 42, no. 33, p. 335 403, 2009.
- [31] D. Sjöberg, M. Gustafsson, and C. Larsson, "Physical bounds on the all-spectrum transmission through periodic arrays: Oblique incidence," *EPL (Europhysics Letters)*, vol. 92, no. 3, p. 34 009, 2010.
- [32] M. Gustafsson and D. Sjöberg, "Sum rules and physical bounds on passive metamaterials," *New Journal of Physics*, vol. 12, no. 4, p. 043 046, 2010.
- [33] R. Mittra, C. H. Chan, and T. Cwik, "Techniques for analyzing frequency selective surfaces-a review," *Proceedings of the IEEE*, vol. 76, no. 12, pp. 1593–1615, 1988.
- [34] M. M. Schiffer and G. Szego, "Virtual mass and polarization," in *Bulletin of the American Mathematical Society*, vol. 54, pp. 130–205, 1948.
- [35] M. Camacho, R. Boix, and F. Medina, "Computationally efficient analysis of extraordinary optical transmission through infinite and truncated subwavelength hole arrays," *Physical Review E*, vol. 93, no. 6, p. 063 312, 2016.
- [36] A. Ericsson, J. Lundgren, and D. Sjöberg, "Experimental characterization of circular polarization selective structures using linearly single-polarized antennas," *IEEE Transactions on Antennas and Propagation*, vol. 65, no. 8, pp. 4239–4249, 2017.
- [37] G. H. Bryant, *Principles of microwave measurements*. IET, 1993, vol. 5.



ergies, scattering and antenna theory applied to periodic structures, as well as signal processing.



Johan Lundgren received his M.Sc. degree in engineering physics from Lund University, Sweden, in 2016. He is currently working towards his Ph.D. degree with the Electromagnetic Theory Group at the Department of Electrical and Information Technology, Lund University. His research interests are in electromagnetic scattering, periodic structures, electromagnetic properties of materials and wave propagation.



Casimir Ehrenborg (S'15) received his M.Sc. degree in engineering physics from Lund University, Sweden, in 2014. He is currently a Ph.D. student in the Electromagnetic Theory Group, Department of Electrical and Information Technology, Lund University. In 2015, he participated in and won the IEEE Antennas and Propagation Society Student Design Contest for his body area network antenna design. His research interests include small antennas, stored energy, phase and radiation centers, as well as physical bounds.



terests include electromagnetic properties of materials, composite materials, as well as optimal performance bounds and realizations for passive and non-passive electromagnetic systems.



Andreas Ericsson (M'13) received his M.Sc. degree in engineering physics and his Ph.D. degree in electrical engineering from Lund University, Lund, Sweden, in 2013 and 2017, respectively. He was awarded a student paper award at URSI GASS 2014 in Beijing. He is currently working as a research engineer at TICRA, and his research interests are electromagnetic scattering, antennas, electromagnetic properties of materials, frequency and polarization selective structures.



Mats Gustafsson (SM'17) received the M.Sc. degree in Engineering Physics 1994, the Ph.D. degree in Electromagnetic Theory 2000, was appointed Docent 2005, and Professor of Electromagnetic Theory 2011, all from Lund University, Sweden.

He co-founded the company Phase holographic imaging AB in 2004. His research interests are in scattering and antenna theory and inverse scattering and imaging. He has written over 90 peer reviewed journal papers and over 100 conference papers. Prof.

Gustafsson received the IEEE Schelkunoff Transactions Prize Paper Award 2010 and Best Paper Awards at EuCAP 2007 and 2013. He served as an IEEE AP-S Distinguished Lecturer for 2013-15.



B. L. G. Jonsson : Received his Ph.D. degree in electromagnetic theory in 2001 from KTH Royal Institute of Technology, Stockholm, Sweden. He was a postdoctoral fellow at University of Toronto, Canada and a Wissenschaftlicher Mitarbeiter (postdoc) at ETH Zurich, Switzerland. Since 2006 he is with the Electromagnetic Engineering Lab at KTH. He is professor in Electromagnetic fields at KTH since 2015. His research interests include electromagnetic theory in a wide sense, including scattering, antenna theory and nonlinear dynamics.



Daniel Sjöberg Daniel Sjöberg (M'11, SM'17) received the M.Sc. degree in engineering physics and Ph.D. degree in engineering, electromagnetic theory from Lund University, Lund, Sweden, in 1996 and 2001, respectively. In 2001, he joined the Electromagnetic Theory Group, Lund University, where, in 2005, he became a Docent in electromagnetic theory. He is currently a Professor and the Head of the Department of Electrical and Information Technology, Lund University. His research interests are in electromagnetic properties of materials, composite

materials, homogenization, periodic structures, numerical methods, radar cross section, wave propagation in complex and nonlinear media, and inverse scattering problems.